FACILE SYNTHESIS OF CHLORIDE-LESS ZIRCONIUM-BASED METAL-ORGANIC FRAMEWORK (MOF) AS CHROMIUM (VI) REMOVAL VIA PHOTOREDUCTION

Anis Muneerah Shaiful Bahari[1], Nisaa Husnina Zulkifli[1], Azieyanti Nurain Azmin[1], Nurhaswani Alias[2], Siti Azlina Rosli[2,3], Nurliyana Abu Hasan Sazalli[2], Zainovia Lockman[2], Nowshad Amin[4] and Halina Misran[1*]

[1] Nanoarchitectonic Laboratory, Department of Mechanical Engineering, Universiti Tenaga Nasional, Jalan IKRAM-UNITEN, 43000 Kajang, Selangor, Malaysia
[2]School of Materials and Mineral Resources Engineering, Universiti Sains Malaysia, Nibong Tebal, 14300 Penang, Malaysia
[3]Faculty of Applied Sciences, Universiti Teknologi MARA Cawangan Pulau Pinang, Permatang Pauh Campus, Permatang Pauh, 13500 Penang, Malaysia
[4]Institute of Sustainable Energy, Universiti Tenaga Nasional, Jalan IKRAM-UNITEN, 43000 Kajang, Selangor, Malaysia

[*]halina@uniten.edu.my

Abstract. Zirconia based metal-organic framework (Zr-MOF) is widely known as hydro-stable and thermally stable MOF structures. However, general synthesis method of Zr-MOF usually employed chloride-based materials to enhance overall crystallinity. The use of chloride-based compounds may hinder the scale-up production of Zr-MOF as it generates scheduled liquid waste and is generally corrosive. In this study, UiO-66, a Zr-MOF was successfully synthesized for the first time without using chloride ions (Cl^-) at room temperature in an attempt for a "green" and facile synthesis. In this method, metal-organic framework formation at various metal salt (Zr^{2+})-to-DMF ratio in with or without the presence of Cl^- as well as its effect on relative crystallinity of UiO-66 were investigated. Decreasing the Zr^{2+}-to-DMF ratio resulted in increased relative crystallinity (RC) regardless of Cl^-. All samples exhibited X-ray diffraction peaks corresponding to (111), (002) and (022) reflection planes suggesting successful UiO-66 formation. Results obtained in this study suggested that UiO-66 with lower RC exhibited highest photoreduction efficiency of Cr (IV) at ca. 54 % in 5 ppm solution with reduction rate of 0.0028 min^{-1}. Higher RC value was suggested to decrease overall active sites for photoreduction reaction to occur resulting in less photoreduction efficiency.

Keywords: UiO-66, chloride-less, facile, photoreduction, Cr(IV)

Article Info

Received 20th September 2021
Accepted 1st December 2021
Published 20th December 2021
Copyright Malaysian Journal of Microscopy (2021). All rights reserved.
ISSN: 1823-7010, eISSN: 2600-7444

Introduction

Chromium released into the environment from industries are mainly in the form of hexavalent chromium [Cr(VI)], known to be toxic and carcinogenic hence even a small amount of Cr(VI) should be eliminated from industrial effluents. Method for mitigating Cr(VI) includes adsorption, membrane filtration, ion-exchange, electrochemical and electrical reduction [1-3]. Reduction reaction is also used especially in plating process of wastewater treatment, whereby Cr(VI) is reduced to a less toxic and more benign Cr(III) using strong acid [4]. Catalytic reduction of Cr(VI) over a catalyst can also be applied and in recent years, photocatalytic reduction of Cr(VI) had been actively investigated [4]. Upon illumination, a photocatalyst can generate electron-hole pairs. If the photogenerated electrons have adequate potential, they can be reduced from Cr(VI) to Cr(III). Many attempts have been made for Cr(VI) reduction over oxide semiconductors. Therefore, instead of using typical oxide semiconductors like titanium dioxide or zinc oxide, Cr(VI) reduction on semiconducting and highly porous metal-organic framework materials (MOFs) has gained considerable interests in recent years [5-9].

MOFs are a class of commonly used metal-organic framework based porous and crystalline materials with high surface area [8,10]. Owing to their distinct porosity and adsorption ability, MOFs have drawn considerable interest in removing heavy metals [11]. In addition, its dispersion ability in aqueous solution is also an added advantage in removing ions in water; comparable to zeolitic materials such as MCM-41 and MCM-48 but with larger pore size. Furthermore, the unique characteristics of MOFs has intrigued researchers to explore on its ability as sensors of various materials such as small molecules, toxic gases and heavy metal ions [12-14].

UiO-66 is classified as one of MOF materials consisting of 12 Zr-O molecule forming $[Zr_6(OH)_4O_4]^{12+}$ octahedrally arranged metal clusters, linked with 1,4-benzenedicarboxylic acid as the organic bridging molecules giving them the high surface area and high thermal stability properties [9]. Since the discovery, there are several less popular Zr-based MOFs analogous due to their synthesis procedures complexity because of their vast organic linker variations [9]. Zr-based MOFs are considered as reactivity semiconductor nanomaterials that are humidity-stable and highly resistant to various solvents making them favourable as support materials for many applications in fluid and corrosive environments. This is due to highly energetic pseudo-ceramic zirconium oxide (Zr-O) bonds at ca. 753 kJ/mol compared to other metal nodes in MOFs [8,15-20]. Presently, studies on UiO-66 as photocatalyst for carbon dioxide capturing and utilisation, Cr(VI) capturing and reduction has been widely explored [11].

Figure 1 shows the suggested schematic diagram of photocatalytic Cr(VI) reduction by UiO-66 where 1,4-benzenedicarboxylic acid (H_2BDC) or known as terephthalic acid (purple sphere) and Zr-O (dark-blue sphere). Free electrons are needed for Cr(VI) reduction process to occur on an oxide semiconductor. These can be generated by electrons excitation from the valence band (VB) to the conduction band (CB) of the oxide upon photons (with energy equal to or greater than the oxide band gap) absorption [17]. In this study, semiconducting UiO-66 will likely undergo similar free-electrons generation process. However, free-electrons will be generated from the highest occupied molecular orbital (HOMO) to the lowest unoccupied molecular orbital (LUMO) [17]. In general, the energy level of organic linker in MOF is regarded as HOMO, while redox potential energy level of Zr-O as metal oxide cluster is regarded as LUMO [17]. Hence, excitation would likely to occur in the organic

linkers. Unlike oxide semiconductors, MOFs are known to be a good adsorbent material thus facilitating more Cr(VI) ions to be adsorbed on the pore surfaces. When illuminated, free electrons from the MOFs may reduce the adsorbed Cr(VI) via electrons transfer resulting in Cr(III) formation. Such synergistic effect may result in a higher efficiency material for Cr(VI) removal from wastewater.

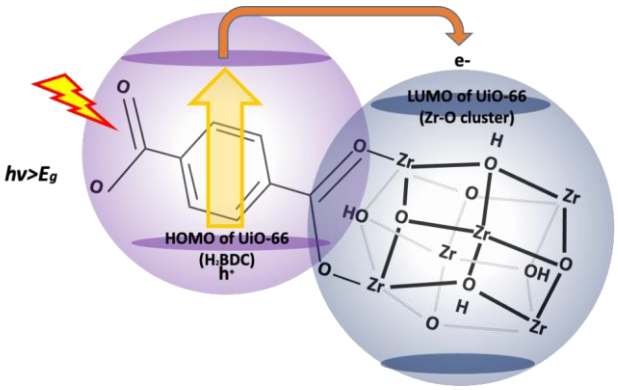

Figure 1. Suggested schematic diagram of the photocatalytic Cr(VI) reduction by adsorption-photoreduction mechanism in UiO-66

However, the majority of synthesis methods in producing UiO-66 employed organic solvents that served as modulators such as dimethylformamide (DMF) and hydrochloric acid (HCl) that hindered their scale-up production due to sheer amount of scheduled liquid waste generation and its high cost [21, 22]. Hence, to the best of our knowledge, all previous studies used DMF in the presence of Cl^- ion in order to successfully obtain UiO-66 as shown in Table 1 [20, 21, 23-29]. However, an initiative to substitute the use of DMF in synthesizing UiO-66 by Venturi *et al*. exhibited successful formation of UiO-66 without DMF in the synthesis system [30]. Thus, in this study, the method was further modified to focus on the effect of Cl^- ion in the system for successful formation of UiO-66. Several studies reportedly used hydrochloric acid (HCl) while others considered Cl^- ion in the metal salts used were enough to cause UiO-66 crystallinity. DMF and HCl are both known as good modulators/solvents to obtain better crystallinity and high surface area of MOF [22]. It was reported that the increased crystallinity in MOFs causes surface area to decrease, as well as the number of active sites on material, consequently affecting its catalytic activity [31].

Table 1. Previous study on UiO-66

References	Years of publication	DMF	Presence of Cl ion	Other solvents
Cavka et. al. [21]	2008	√	√	x
Cirujano et. al. [23]	2015	√	√	dichlorometane
Piscopo et. al. [24]	2015	√	√	Methanol
Lan et. al. [25]	2016	√	√	x
Zhang et. al. [20]	2017	√	√	x
Caratelli et. al. [26]	2017	√	√	dichlorometane
Torbina et. al. [27]	2019	√	√	x
Liu et. al. [28]	2019	√	√	Acetic acid
This study	2021	√	x	x

Therefore, in this study, UiO-66 was synthesized with different metal salt/DMF ratios and aging durations. The study of metal salts to organic linkers ratio and without Cl^- ion (chloride-less) was carried out as an initiative to decrease the use of acid modulators. The effect of these parameters on the resultant crystallinity of UiO-66 was also investigated. Furthermore, UiO-66 synthesized without Cl^- used as photocatalyst for adsorption-photoreduction of Cr(VI) ions from water were also elucidated in this study.

Methods and Materials

Materials. Zirconium (IV) oxynitrate hydrate (N_2O_7Zr, Fluka), terephthalic acid ($C_8H_6O_4$, 1,4-benzenedicarboxylic acid, H_2BDC, Merck, 98%), N, N-dimethylformamide (DMF, Merck, 99.8%), hydrochloric acid (HCl, Fluka, 99%) and distilled deionized water were used for the synthesis. Potassium dichromate ($K_2Cr_2O_7$) was used for Cr (VI) solution. All reagents were used in as-received condition without further purification.

Synthesis. UiO-66 was synthesized using reported methods with some modifications [24,28]. Terephthalic acid was dissolved in DMF and sonicated for 10 minutes. Then, zirconium salt was added to the organic solution with 0.099 mol of HCl and sonicated again for several minutes. The resulting solution was placed into Teflon-lined stainless steel autoclave, aged overnight and cooled to room temperature. The solution was centrifuged, thoroughly washed with DMF and acetone then activated by heating at several drying conditions in vacuo as shown in Table 2. The synthesis was repeated for chloride-less synthesis omitting the addition of HCl with two-stages drying conditions. Water was not used for washing all those samples to prevent the possibility of hydrolytic cleavage occurrence. The resultant precipitates were dried in vacuo. The initial pH of the mixtures without using HCl were less than 5.5 whereby above that will cause the organic linker molecule to be released again into the solution and fail to form metal-organic framework structure [4,33].

Table 2. Synthesis parameters of UiO-66 with or without Cl^-

Sample	Zr^{2+}: DMF	Cl^-	Aging duration (h)	Dry
UiO-66(1)	1:270	Yes	24	80°C, 6h
UiO-66(2)	1:270	Yes	48	80°C, 6h
UiO-66(3)	1:200	No	24	90°C, 1h; 120°C, 5h
UiO66(4)	1:200	Yes	24	80°C, 6h
UiO-66(5)	1:400	No	24	90°C, 1h; 120°C, 5h
UiO-66(6)	1:400	Yes	24	80°C, 6h

Structural Characterizations. X-ray diffraction (XRD) patterns were determined using Shimadzu XRD-6000 at 30 kV, 20 mA, scan step of 0.02°, scan speed 3°/min at $2\theta = 5^o – 45^o$ [34,35]. The primary particle size was estimated using Scherrer equation and Williamson and Hall (WH) method. In WH method, the size broadening and strain broadening were taken

into consideration. The uniform deformation model (UDM) model of WH plot can be expressed as [36]:

$$\beta \cos \theta = 4C_{\varepsilon} \sin \theta + k\lambda/D \quad (1)$$

where C_{ε} is the value of strain, β is the FWHM value in radian, θ is the Bragg diffraction angle in radian, K is a constant due to shape factor (0.9) and λ is the wavelength of the incident X-ray used (1.5406 Å). β cos θ as Y-axis is plotted against 4 sin θ as X-axis, forming linear Lorentzian profiles. The crystallite size is calculated using the value of the intercept formed. Relative crystallinity (RC) values were calculated using the relative intensity of highest sample taken as 100 %. Hitachi SU8020 Field Emission Scanning Electron Microscopy (FESEM) was used to observe the morphology of samples at 15 kV acceleration voltage. Thermogravimetric analysis (TGA) was done using Shimadzu DTG-60 at 10°C/min, as nitrogen gas flow at 100 ml/ minute in Pt pans from 25°C to 900°C [35]. Fourier transform infrared spectroscopy (FT-IR) analyses were done using IRPrestige-21 Shimadzu at 500 cm^{-1} - 4000 cm^{-1} wavenumber. Raman spectroscopy was carried out to identify the chemical composition using RENISHAW in via Raman microscope with an excitation wavelength of 532 nm and 1% laser power. Nitrogen adsorption-desorption analysis was done using Micromeritics ASAP2050XP at -196°C. Surface area, pore volume and pore size distribution were estimated using BET and Langmuir method. Pore size distribution were determined using both Horvath–Kawazoe (HK) method for micropore and BJH method for mesopore. Prior to nitrogen adsorption, the samples were pre-treated by degassing at 150°C for 24 h.

Photoreduction of Cr(VI) ions from aqueous solution. Solution 1 of Cr(VI) was prepared using potassium dichromate ($K_2Cr_2O_7$) dissolved in deionized water to produce 100 ppm Cr(VI) solution with an initial pH of 4. Then, the Solution 1 was further diluted to 5 ppm and pH was adjusted to 2 by adding HCl to produce Solution 2. Then, 0.05 g of UiO-66 powders were packed in a tea-bag and immersed in 25 ml of Solution 2. Before light irradiation, UiO-66 in Solution 2 was left in the dark for ca. 30 mins to achieve adsorption–desorption equilibrium. The solution was then exposed to UV light for 300 mins. The amount of Cr(VI) left in Solution 2 (after photoreduction) was observed by taking out 5 ml of the solution at 30 mins intervals. Then, the solution's UV absorbance was measured at 350 nm using UV-visible spectroscopy (Perkin Elmer Lambda 35). Excess electrons are needed for complete reduction from Cr(VI) to Cr(III) ion as shown in the following equation [9]:

$$Cr_2O_7^{2-} + 14H^+ + 6e^- \rightarrow 2Cr^{3+} + 7H_2O \quad (2)$$

The removal efficiency (E, %) was estimated according to equation:

$$E\ \% = (C_0 - C_t)/C_0 \times 100\% \quad (3)$$

where, C_0 and C_t are the initial and final concentration of Cr(VI) ions in (mg/L), respectively. The UV light (Hitachi F8T5-Black Light, 8 Watts) energy used was 3.4 eV, which is higher than UiO-66 band gap (3.05 eV) [17]. Hence, photogenerated electrons can be expected. The kinetic reaction was then calculated using the pseudo-first-order Langmuir Hinshelwood model [37]:

$$R = -dC/dt = kt \quad (4)$$

When the adsorption is weak, this can be expressed as:

$$-\ln(C/C_0) = kt \quad (5)$$

where R is the photocatalytic reaction rate, k is the photocatalytic pseudo-first order reaction rate constant, C is the concentration of Cr(VI) at the given time and C_0 is the initial concentration of Cr(VI).

Results and Discussion

Characterizations. UiO-66 produced without Cl^- gave higher yield at ca. 60% more powder compared to other samples. Figure 2 shows the XRD patterns of UiO-66 (1) to UiO-66 (6). All samples exhibited nine prominent peaks at 2θ = 7.3°, 8.4°, 12°, 17°, 22.1°, 25.6°, 30.6°, 37.4° and 43.3° which corresponds to (111), (200), (220), (040), (511), (600), (711), (751) and (400) crystal planes. The existence of these peaks with highest peak observed at (111) plane of octahedral facets suggested successful formation of UiO-66 with octahedral structure [21,32]. However, the samples synthesized using Cl^-; UiO-66 (1), UiO-66 (2), UiO-66 (4) and UiO-66 (6) exhibited an additional reflection peak at 2θ = 25.3° corresponding to (101) crystal plane attributed to free, non-framework ZrO_2 phase [38].

Crystallinity in terms of relative crystallinity (RC) values were calculated with 100% crystallinity referenced to sample UiO-66 (1) for having highest (111) reflection plane. Table 3 shows the crystallite size and RC of UiO-66 samples. UiO-66 (2), UiO-66 (3), UiO-66 (4), UiO-66 (5) and UiO-66 (6) have a RC of 66%, 56%, 73%, 50% and 96%, respectively. XRD patterns of UiO-66 (1) and UiO-66 (2) that were aged at two different durations suggested that aging at 24 h is sufficient for the formation of highly crystalline UiO-66. Even though, XRD pattern suggested that aging for 24 h yielded higher crystallinity, it was reported that the changes in UiO-66 main peak may vary and does not depend on the aging duration [32]. Therefore, samples that were prepared without Cl^- (UiO-66 (3) and UiO-66 (5)) resulted in lower RC value at ca. 56% and ca. 50%, respectively. This finding suggested that the presence of Cl^- is important to improve crystallinity [27, 32].

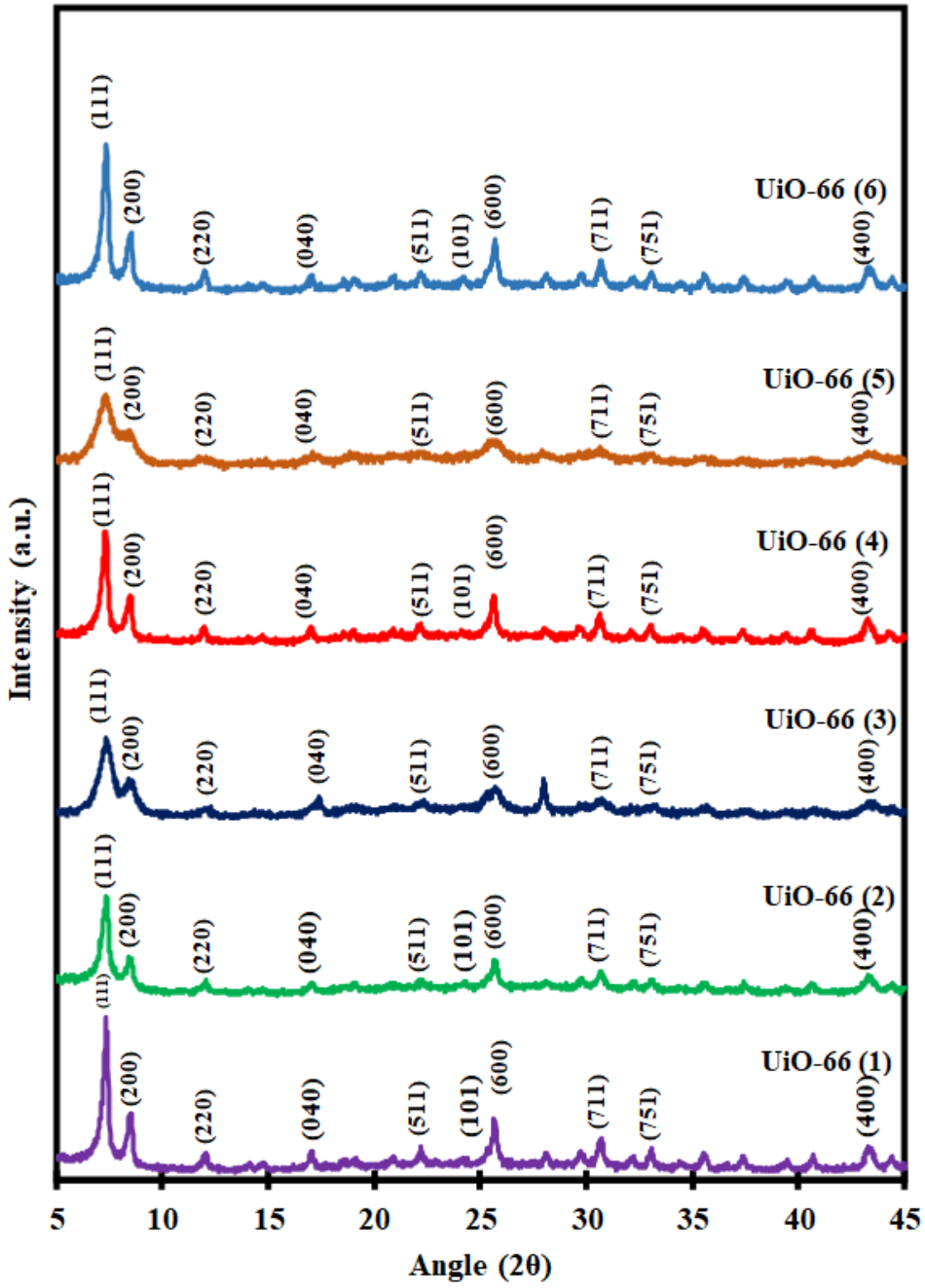

Figure 2. X-ray diffraction patterns of as-synthesized UiO-66

Table 3. Relative Crystallinity (RC) and crystallite size of the synthesized UiO-66

UiO-66	Relative Crystallinity (RC)	Crystallite size (nm) by Scherrer equation	Crystallite size (nm) by WH plot
1	100%	26	29
2	66%	19	20
3	56%	10	10
4	73%	22	24
5	50%	8	9
6	96%	23	26

The primary crystallite size was calculated using Scherrer equation was at a range of ca. 8 nm to 26 nm. The estimated crystallite size calculated shows a similar value with grain observed in WH plot (Figure 3) with a range of ca. 9 nm to 29 nm. Samples without Cl^-; UiO-66 (3) and UiO-66 (5) showed smallest crystalline sizes of 10 nm and 8 nm as well as low crystallinity suggesting that the small particles formed loose agglomerations giving rise to porous structure. However, the samples synthesized with Cl^-, which are UiO-66 (1), UiO-66 (2), UiO-66 (4) and UiO-66 (6) exhibited larger primary crystallite sizes of ca. 26, 19, 22 and 23 nm, respectively. Thus, in the presence of Cl^- bigger crystallites were observed while the Zr^{2+}/DMF ratio had no apparent effect on the crystallite size.

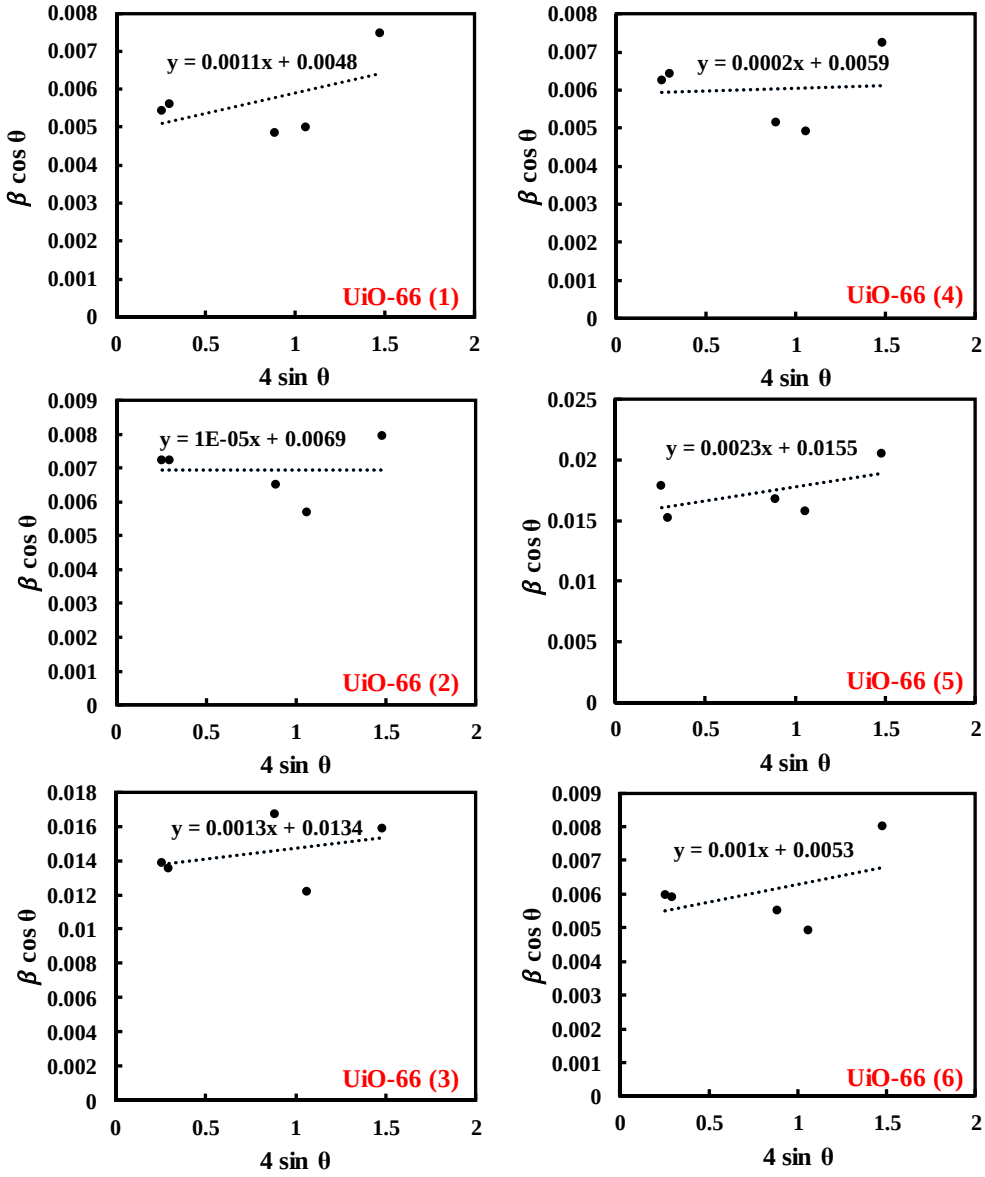

Figure 3. The Williamson-Hall (W-H) plots of synthesized UiO-66

Figure 4 shows FESEM images of dried UiO-66 (1), UiO-66 (3), UiO-66 (4) and UiO-66 (6). UiO-66 was known to form octahedral structure but the cubic ingrown crystal was also observed [32]. UiO-66 (1) shows cubic ingrown morphology with good crystallinity, as reported in previous study [32]. Furthermore, UiO-66 (6) and UiO-66 (4) were expected to produce a similar cubic ingrown structure as UiO-66 (1) but cubic ingrown shapes were not defined as observed in UiO-66 (1). On the other hand, without Cl^- sample, UiO-66 (3) exhibited agglomerations of cubic ingrown crystals but with less defined structure than in sample with Cl^-, UiO-66 (4). It was assumed that the primary crystal may agglomerate to form porous structure as observed in FESEM. The FESEM images corresponds well to the XRD results suggesting that Cl^- affected the overall crystallinity of resultant UiO-66. Structural results suggested that Zr^{2+}/DMF ratio must be optimum in value so as not to be less or more than 1:270 in UiO-66 (1) in order to obtain high UiO-66 crystallinity.

Figure 5 shows the thermal stability of UiO-66 (1), UiO-66 (3), UiO-66 (4) and UiO-66 (6). All of the samples decomposed in three-stages of weight loss. The first weight loss was at ca. less than 10 % before 100°C due to solvent's evaporation. Then, between 100°C and 300°C, second weight loss at ca. 30 % occurred due to loss of water molecules physisorbed in the structure. Third weight loss occurred at 600 °C at ca. 25 % mass reduction due to the decomposition of organic molecules, which left ZrO_2 as final residual oxides [21].

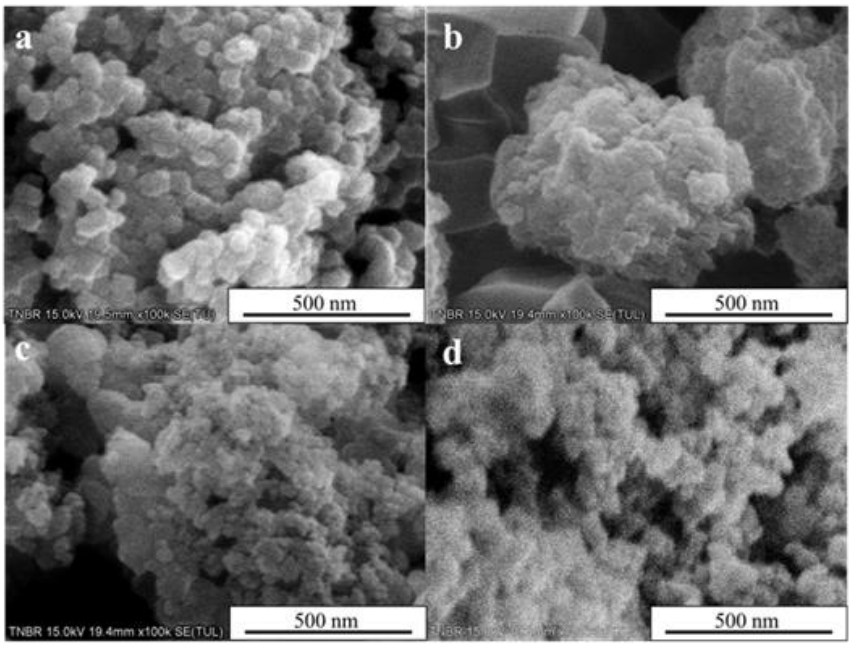

Figure 4. FESEM images of UiO-66 a) UiO-66 (1) b) UiO-66 (3) c) UiO-66 (4) and d) UiO-66 (6)

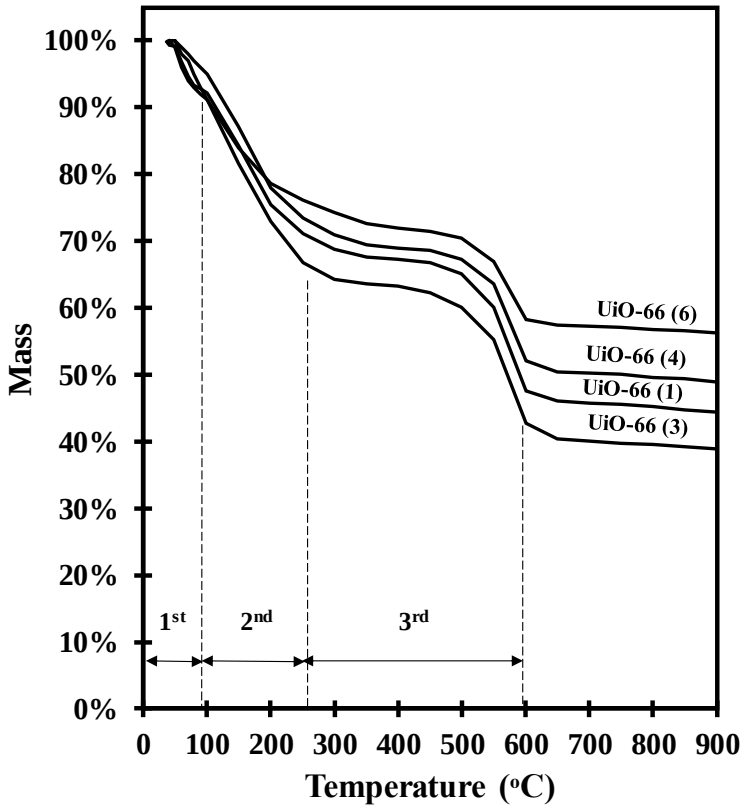

Figure 5. Thermal stability of UiO-66 (1), UiO-66 (3), UiO-66 (4) and UiO-66 (6)

Figure 6 shows that FT-IR spectra exhibited characteristic peaks attributable to the vibration of C–H bonds in aromatic compound at frequencies of 2972 cm^{-1}, 2879 cm^{-1} and 1880 cm^{-1} were observed. The vibration of C-O bonds was observed as two strong peaks at 1087 cm^{-1}, 1045 cm^{-1} and one weaker peak at 1379 cm^{-1} originating from terephthalic acid. The adsorption band at 655 cm^{-1} corresponds to Zr-O stretching frequency as reported [20, 21, 27, 39]. As observed in Figure 7, UiO-66 synthesized in this study exhibited Raman shift at 863 cm^{-1}, 1140 cm^{-1}, 1430 cm^{-1}, 1450 cm^{-1} and 1615 cm^{-1} which corresponds to UiO-66 structure in previous study [40].

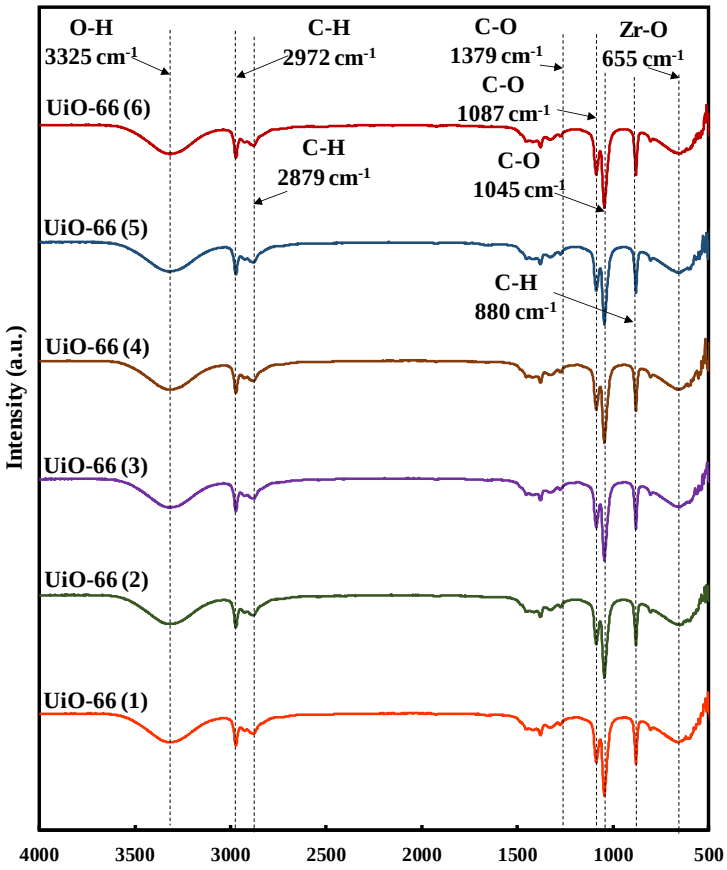

Figure 6. FT-IR spectra of synthesized UiO-66

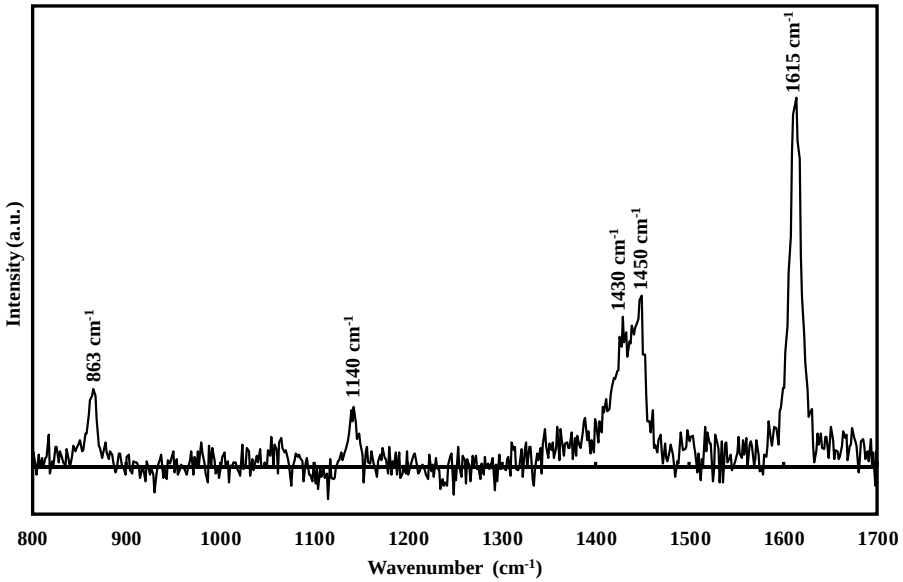

Figure 7. Representative Raman spectrum of synthesized UiO-66 (4)

Porosity characteristics. Porosity characteristics such as size and surface also influence the accessibility of reactants to the active sites and the ability of diffusing products back into bulk fluid. Figure 8 shows a representative adsorption-desorption isotherm of as-

synthesized, non-activated UiO-66 (5) prepared without Cl^-. The insets are median pore size distribution determined by Horvath-Kawazoe (HK) and Barret-Joyner- Halenda (BJH) method. The adsorption isotherm of UiO-66 (5) exhibited the combination of Type 1b and type IVb with the presence of hysteresis loop at the desorption branch suggesting the dual nature of microporous and mesoporous material. Unlike typical UiO-66 materials that exhibited purely Type 1a isotherm of microporous structure, the samples prepared in this study exhibited Type 1b structure suggesting that a stable and undistorted formation of monolayer range on the walls of wider micropore (cooperative filling). The surface area estimated using BET and Langmuir was at ca. 400 m^2/g. In general, metal-organic framework materials give Type IVb with hysteresis of H2 loop observed for adsorption by network-percolation effect [41]. The blue inset shows the median pore size distribution (PSD) centered at ca. 0.7 nm determined by HK method in agreement with the concept of wider micropore filling observed for Type 1b isotherm. The brown inset represents median pore size distribution by the BJH method for mesopore centered at ca. 3.5 nm suggesting the presence of wider mesoporous compared to typical mesoporous materials at ca. 2 - 3 nm [42]. It can be assumed that other synthesized UiO-66 has a lower pore size, surface area and concentration of active sites compared to UiO-66 (5).

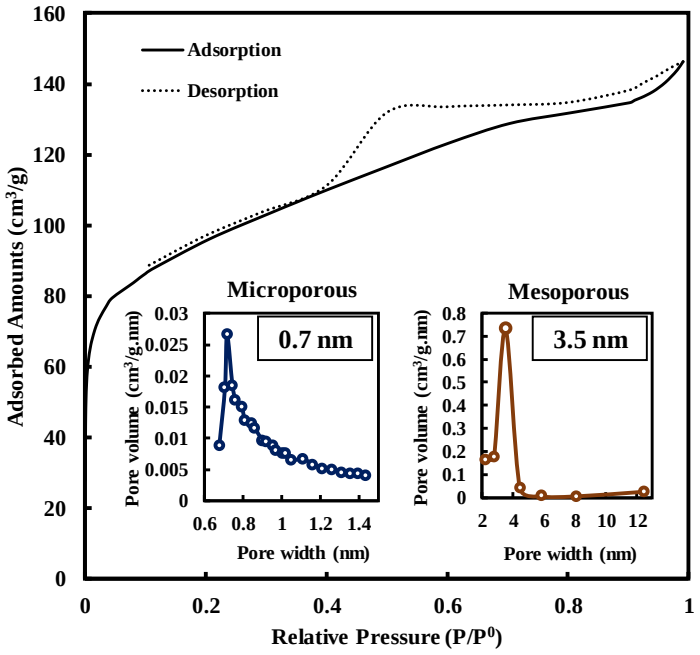

Figure 8. N_2 adsorption isotherm and pore size distribution (inset) of a representative UiO-66 (5)

Photoreduction of Cr(VI) ion from aqueous solution. Figure 9 (a) shows the removal of Cr(VI) ion in the presence of UiO-66 (1), UiO-66 (4) and UiO-66 (5). These three samples were selected due to their variety of RC values being highest, medium and lowest. Photoreduction efficiency as shown in Figure 9 a) suggested that lower RC exhibited highest removal of Cr(VI) ion. UiO-66 (1) removed ca. 12 % of Cr(VI), UiO-66 (4) 27 % and UiO-66 (5) 54 % even after 5 hours of UV irradiation. The increase in Cr(VI) removal efficiency was suggested due to the decrease in particle size and crystallinity of UiO-66. UiO-66 crystallinity reduction resulted in an increase in amorphous structure and surface area [42]. This increase leads to increment of active sites on the surface to catalyze photoreduction [39].

The photoreduction active sites in amorphous structure are zirconium oxide clusters which provides wider contact area for the reaction to occur [31].

The values obtained in this study were considerably small as compared to UiO-66 produced using Cl^- as reported before, with the removal efficiency of 5 ppm Cr(VI) ion at ca. 45% and above achieved in 45 minutes [7]. Nevertheless, in this study, the formation of UiO-66 without using Cl^- is new and can be considered as sustainable approach in the attempt of cost reduction and upscaling the production of MOFs.

The larger contact areas and more active sites may be provided by amorphous particles agglomerating with irregular porous structures as suggested by FESEM images obtained in this study [31,43]. In general, strategic approaches to enlarge the surface area of the adsorbent and thereby improve the efficiency of photoreduction requires the reduction of particle size [31]. This finding suggested that lower RC exhibited higher photoreduction of Cr(VI). Moreover, the results obtained in this study was in good agreement to UiO-66 (5) prepared without Cl^- achieving 54 % photoreduction efficiency. Moreover, the sample exhibited ca. 50 % of Cr(VI) ions reduction achieved at ca. 180 min after UV exposure. Thereafter, additional 4% decrease was observed from 180 to 300 min. However, for UiO-66 (1) and UiO-66 (4) photoreduction occurred at a very slow rate with overall photoreduction efficiency of ca. 25 % and ca. 10 %.

Figure 9 b) shows the UV-Vis results of UiO-66 (5) taken at 30 mins time interval. The absorbance peak corresponding to Cr(VI) ions was observed at ca. 350 nm. The reduction in peak intensity from 0 – 300 mins suggested that Cr(VI) ions were successfully removed from the solution by photoreduction. In order to ensure that reduction occur by photoreduction, UiO-66 (5) samples in Solution 2 was left in the dark for 300 mins as shown in Figure 9 c) exhibiting ca. 5 % in removal efficiency, suggesting that the reduction in Cr(IV) ion using samples in this study occurred purely by photoreduction. The removal efficiency of Cr(VI) in dark experiment occurred purely by adsorption and was negligible.

Therefore, it can be concluded that the Cr(VI) removal was carried out via photoreduction for free electrons generation to initiate reduction from Cr(IV) to Cr(III). This was not caused by adsorption alone as it was inadequate for efficient removal. Nevertheless, much ought to be investigated in order to further understand the synergistic effect of both processes on UiO-66.

Figure 10 shows the graph of $-\ln(C/C_0)$ vs. time. The inset are k values and R^2 values for Cr(VI) ions. The values of photocatalytic pseudo-first-order reaction rate constant (k) and the correlation coefficient of determination (R^2) were calculated. The value of k is the slope of the linear fit. Also, the value of R^2 must be close to 1, indicating that the model is suitable for illustrating Cr(VI) kinetics. Based on the value of k obtained in Figure 10, the photocatalytic activity of UiO-66 (4) is almost three times higher at $k = 0.0011$ min^{-1} than UiO-66 (1) with k value of 0.0004 min^{-1}. However, UiO-66 (5) with the lowest RC shows the highest value of k compared to other UiO-66 samples. These results suggested that the pseudo-first-order Cr(VI) reaction rate constant increases when the RC decreases.

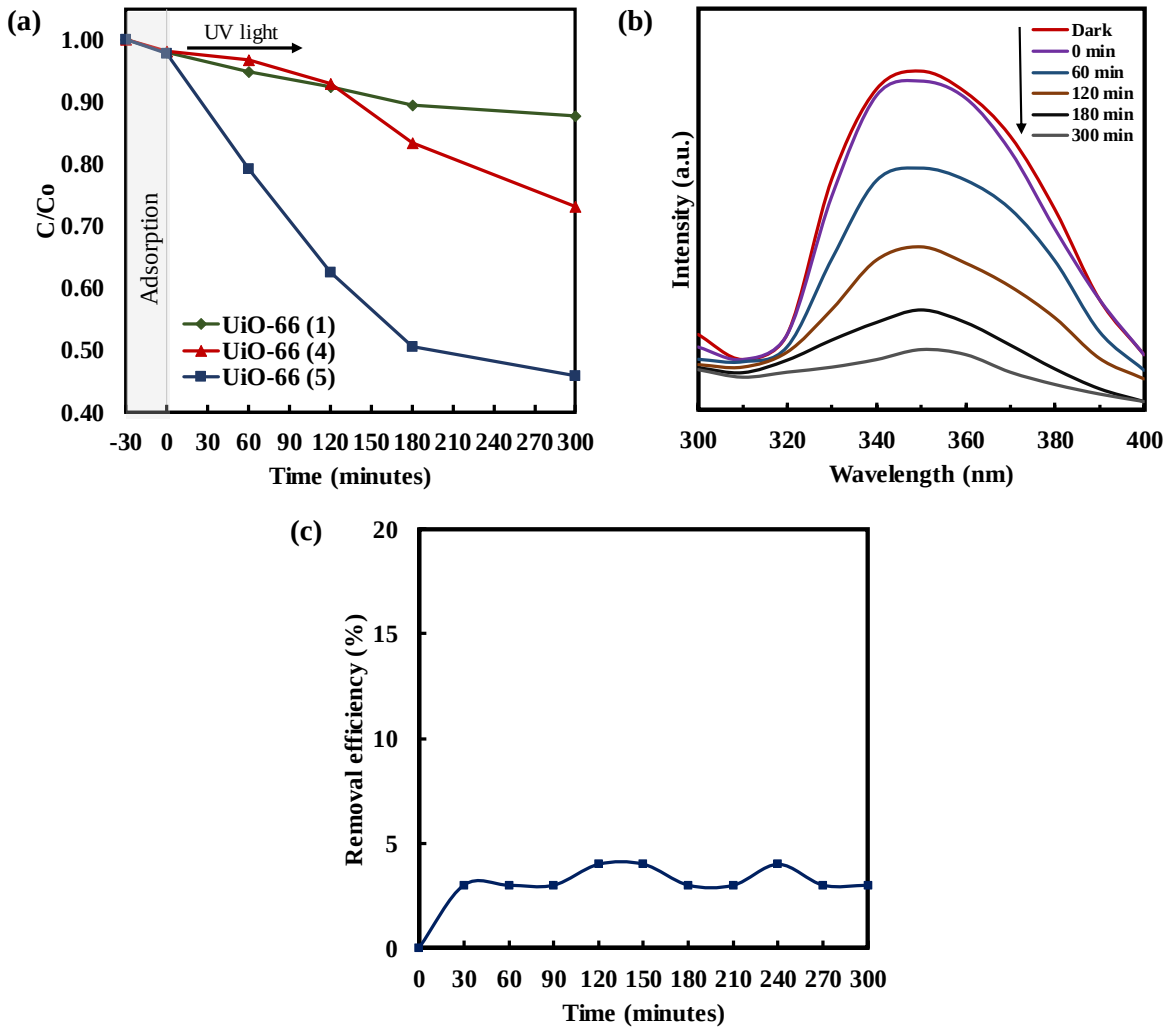

Figure 9. Photoreduction efficiency of Cr(VI) ion by UiO-66 b) UV-Vis result of UiO-66 (5) and c) removal efficiency of Cr(VI) by UiO-66 (5) in dark

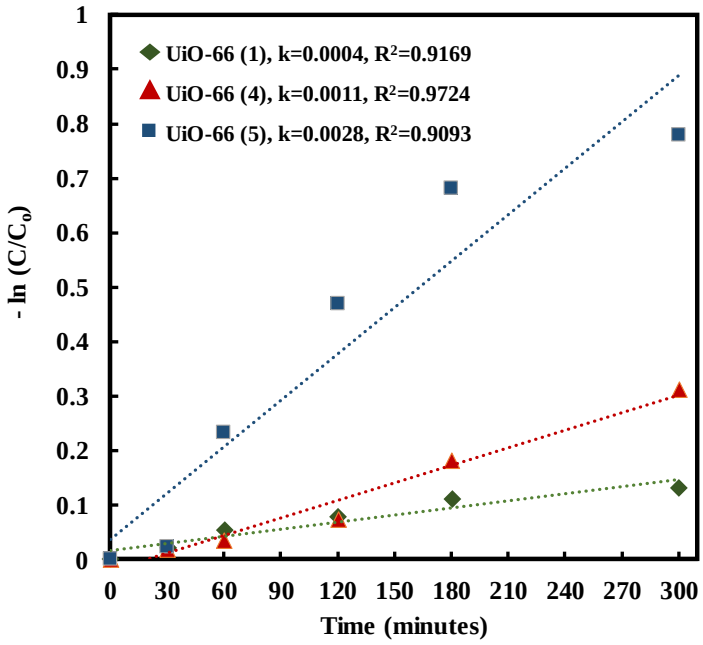

Figure 10. Graph of –ln(C/C$_0$) vs. time and the reduction rate contants for UiO-66 (1), UiO-66 (4) and UiO-66 (5)

Conclusion

UiO-66 with varying RC were successfully synthesized with or without Cl^- at different aging and drying conditions. Crystallinity was improved by adding Cl^-. However, results suggested that for photoreduction removal efficiency requires lower crystallinity. It was suggested that lower crystallinity can lead to a higher surface area which may increase the active sites catalyzing the photoreduction reaction on the material's surface. Nevertheless, the sample had to be illuminated as to induce photogenerated electrons for the reduction of Cr(VI) to take place. While the efficiency could be further improved, synthesizing UiO-66 without using HCl is a high yielding new and sustainable approach in the attempt to scale-up production of MOFs and reduction of byproducts.

Acknowledgements

The authors thank Universiti Tenaga Nasional for Postgraduate Excellence Scholarship (No: UNITEN/CBDO(MSA) 1/14/1) BOLD grant, No: RJO10517844/115 and J510050002/2021083. A.M.S. Bahari thanks Universiti Sains Malaysia (USM) for providing photoreduction facilities.

Author contributions

All authors contributed toward data analyses, drafting and critically revising the paper and agree to be accountable for all aspects of the work.

Disclosure of conflict of interest

The authors have no disclosure of conflict of interest.

Compliance with ethical standards

The work is compliant with ethical standards.

References

[1] Wen, J., Fang, Y., & Zeng, G. (2018). Progress and Prospect of Adsorptive Removal of Heavy Metal Ions from Aqueous Solution Using Metal–Organic Frame-works: A Review of Studies from the Last Decade. *Chemosphere,* 201 627-643

[2] Barakat, M. A. (2011). New Trends in Removing Heavy Metals from Industrial Wastewater. *J. Chem,* 4 361-377

[3] Lockman, Z. (2019). *1-Dimensional Metal Oxide Nanostructures* (CRC Press)

[4] Wahyuni, E. T., Aprilita, N. H., Hatimah, H., Wulandari, A. M., & Mudasir, M. (2015). Removal of Toxic Metal Ions in Water by Photocatalytic Method. *J. Am. Chem., Soc.* 5 194-201

[5] Pakade, V. E., Tavengwa, N. T., & Madikizela, L. M. (2019). Recent Advances in Hexavalent Chromium Removal from Aqueous Solutions by Adsorptive Methods. *RSC Adv*., 9 26142-26164

[6] Noraee, Z., Jafari, A., Ghaderpoori, M., Kamarehie, B., & Ghaderpoury, A. (2019). Use of Metal-Organic Framework to Remove Chromium (VI) from Aqueous Solutions. *J. Environ. Health Sci. Eng*., 17 701-709

[7] Jiang, C., Sun, R., Du, Z., Singh, V., & Chen, S. (2020). A Cationic Zr-Based Metal Organic Framework with Enhanced Acidic Resistance for Selective and Efficient Removal of CrO_4^{2-}. *New J. Chem.,* 44 12646-12653

[8] Saiz, P. G., Valverde, A., Gonzalez-Navarrete, B., Rosales, M., Quintero, Y. M., Fidalgo-Marijuan, A., Orive, J., Reizabal, A., Larrea, E. S., Arriortua, M. I., Lanceros-Méndez, S., García, A., & Luis, R. F. D. (2021). Modulation of the Bifunctional CrVI to CrIII Photoreduction and Adsorption Capacity in Zr IV and Ti IV Benchmark Met-al-Organic Frameworks. *Catalysts*, 11 51-65

[9] Shokouhfar, N., Aboutorabi, L., & Morsali, A. (2018), Improving the Capability of UiO-66 for Cr(vi) Adsorption from Aqueous Solutions by Introducing Isonicotinate: N -Oxide as the Functional Group. *Dalton Trans.,* 47 14549-14555

[10] Zhou, H. C., Long, J. R., & Yaghi, O. (2012). Introduction to Metal–Organic Frameworks. *Chem. Rev.,* 112 673-674

[11] Kumar, P., Pournara, A., Kim, K. H., Bansal, V., Rapti, S., & Manos, M. J. (2017). Metal-Organic Frameworks: Challenges and Opportunities for Ion-Exchange/Sorption Applications. *Prog. Mater. Sci.,* 86 25-74

[12] Kaur, H., Sinha, S., Krishnan, V., & Koner, R. R. (2020). Photocatalytic Reduction and Recognition of Cr(VI): New Zn(II)-Based Metal–Organic Framework as Catalytic Surface. *Ind. Eng. Chem. Res.,* 59 8538-8550

[13] Stanley, P. M., Haimerl, J., Thomas, C., Urstoeger, A., Schuster, M., Shustova, N. B., Casini, A., Rieger, B., Warnan J., & Fischer, R. A., (2021). Host–Guest Interactions in a Metal–Organic Framework Isoreticular Series for Molecular Photocatalytic CO_2 Reduction. *Angew. Chem. Int. Ed*., 60 17854-17860

[14] Li, D., Kassymova, M., Cai, X., Zang, S. Q., & Jiang, H. L. (2020). Photocatalytic CO_2 Reduction over Metal-Organic Framework-based Materials. *Coord. Chem. Rev.,* 412 213262

[15] Luo, Y.R. (2007). *Comprehensive Handbook of Chemical Bond Energies* (CRC Press)

[16] Silva, C. G., Corma, A., & García, H. (2010). Metal-Organic Frameworks as Semiconductors. *J. Mater. Chem.,* 20 3141-3156

[17] Li, R., Zhang, W., & Zhou, K. (2018). Metal–Organic-Framework-Based Catalysts for Photoreduction of CO_2. *Adv. Mater*., 35 1705512-1705543

[18] Nasalevich, M. A., Veen, M. V. D., Kapteijn, F., & Gascon, J. (2014). Metal-organic frameworks as heterogeneous photocatalysts: Advantages and challenges. *Cryst. Eng. Comm.,* 16 4919-4926

[19] Li, J., Musho, T., Bright, J., & Wu, N. (2019). Functionalization of a Metal-Organic Framework Semiconductor for Tuned Band Structure and Catalytic Activity. *J. Electrochem. Soc*., 5 H3029-H3034

[20] Zhang, X., Huang, P., Liu, A., & Zhu, M. (2017). A Metal–Organic Framework for Oxidative Desulfurization: UiO-66(Zr) as a Catalyst. *Fuel*, 209 417-423

[21] Cavka, J. H., Jakobsen, S., Olsbye, U., Guillou, N., Lamberti, C., Bordiga, S., & Lilerud, K. P. (2008). A New Zirconium Inorganic Building Brick Forming Metal Organic Frameworks with Exceptional Stability. *J. Am. Chem. Soc.,* 130 13850-13851

[22] Hu, Z., & Zhao, D. (2015). Methodologies toward the Synthesis and Scale-up Production of UiO-66-Type Metal-Organic Frameworks and Membrane Materials. *Dalton Trans.,* 44 19018-19040

[23] Cirujano, F. G., Corma, A., & Llabrés i Xamena, F. X. (2015). Conversion of Levulinic Acid into Chemicals: Synthesis of Biomass Derived Levulinate Esters over Zr-Containing MOFs. *Chem. Eng. Sci.,* 124, 52-60

[24] Piscopo, C. G., Polyzoidis, A., Schwarzer, M., & Loebbecke, S. (2015). Stability of UiO-66 under Acidic Treatment: Opportunities and Limitations for Post-Synthetic Modifications. *Micropor. Mesopor. Mat.,* 208, 30-35

[25] Lan, X., Zhang, H., Bai, P., & Guo, X. (2016). Investigation of Metal Organic Frameworks for the Adsorptive Removal of Hydrochloride from Dilute Aqueous Solution. *Micropor. Mesopor. Mat.,* 231 40-46

[26] Caratelli, C., Hajek, J., Cirujano, F. G., Waroquier, M., Llabrés i Xamena, F. X., & van Speybroeck, V. (2017). Nature of Active Sites on UiO-66 and Beneficial Influence of Water in the Catalysis of Fischer Esterification. *J. Catal*., 352 401-414

[27] Torbina, V. V., Nedoseykina, N. S., Ivanchikova, I. D., Kholdeeva, O. A., & Vodyankina, O. V. (2019). Propylene Glycol Oxidation with Hydrogen Peroxide over Zr-Containing Metal-Organic Framework UiO-66. *Catal. Today,* 333 47-53

[28] Liu, L., Xie, X., Qi, S., Li, R., Zhang, X., Song, X., & Gao, C. (2019). Thin Film Nanocomposite Reverse Osmosis Membrane Incorporated with UiO-66 Nanoparticles for Enhanced Boron Remo-val. *J. Membr. Sci*., 580 101-109

[29] Kim, T. H., & Kim, S. G. (2011). Clinical Outcomes of Occupational Exposure to N,N-Dimethylformamide: Perspectives from Experimental Toxicology. *Saf. Health Work,* 2 97-104

[30] Venturi, D. M., Campana, F., Marmottini, F., Costantino, F., & Vaccaro, L. (2020). Extensive Screening of Green Solvents for Safe and Sustainable UiO-66 Synthesis. *ACS Sustain. Chem. Eng.,* 8 17154−17164

[31] Wang, C., Liu, X., Chen, J. P., & Li, K. (2015). Superior Removal of Arsenic from Water with Zirconium Metal-Organic Framework UiO-66. *Sci. Rep.,* 5 1-10

[32] Rahmawati, I. D., Ediati, R., & Prasetyoko, D. (2014). Synthesis of UiO-66 Using Solvothermal Method at High Temperature. *IPTEK Journal of Proceedings Series,* 42-46

[33] Buzek, D., Adamec, S., Lang, K., & Demel, J. (2021). Metal–Organic Frameworks vs. Buffers: Case Study of UiO-66 Stability. *Inorg. Chem Front*., 8 720-734

[34] Misran, H., Othman, S. Z., Manap, A., Fauzi, N. I. M., & Ramesh, S. (2014). Nonsurfactant Synthesis and Characterizations of Metal- Organic Framework MOF-5 Materials Using Fatty Alcohols. *Sci. Adv. Mater.,* 6 1638-1644

[35] Fadli, M. F. M., Misran, H., Othman, S. Z., Bahari, A. M. S., Samsudin, N. A., Rosli, S. A., Lockman, Z., Matsumoto, A., & Amin, N. (2019). Room Temperature Synthesis and Characterizations of CU-MOF Using Natural Polysaccharide as Potential Organic Linker. *J. Recent Technol.,* 8 6490-6498

[36] Pratheepa, M. I., & Lawrence, M. (2021). X-Ray Diffraction Analyses of Titanium Dioxide Nanoparticles. *Int. J. Sci. Res. Sci. Technol.,* 3 83-88

[37] Rosli, S. A., Alias, N., Bashirom, N., Ismail, S., Tan, W. K., Kawamura, G., Matsuda, A., & Lockman, Z. (2021). Hexavalent Chromium Removal via Photoreduction by Sunlight on Titanium–Dioxide Nanotubes Formed by Anodization with a Fluorinated Glycerol–Water Electrolyte. *Catalysts*, 11, 376

[38] Feng, L., Yuan, S., Zhang, L., Tan, K., Li, J., Kirchon, A., Liu, L., Zhang, P., Han, Y., Chabal, Y. J., & Zhou, H. (2018). Creating Hierarchical Pores by Controlled Linker Thermolysis in Multivariate Metal-Organic Frameworks. *J. Am. Chem. Soc*., 6 2363-2372

[39] Fu, Y. Y., Yang, C. X., & Yan, X. P. (2013). Incorporation of Metal-Organic Framework UiO-66 into Porous Polymer Monoliths to Enhance the Liquid Chromatographic Separation of Small Molecules. *ChemComm.*, 49 7162-7164

[40] Otal, E. H., Kim, M. L., Calvo, M. E., Karvonen, L., Fabregas, I. O., Sierra, C. A., & Hinestroza, J. P. (2016). A Panchromatic Modification of the Light Absorption Spectra of Metal–Organic Frameworks. *ChemComm.*, 52, 6665-6668

[41] Rouquerol, F., Rouquerol, J., & Sing, K. (1998). *Adsorption by Powders and Porous Solids* (Academic Press)

[42] Matsumoto, A., Misran, H., & Tsutsumi, K. (2004). Adsorption Characteristics of Organosilica Based Mesoporous Materials. *Langmuir*, 20 7139-7145

[43] Wei, W., Yang, L., Zhong, W., Cui, J., & Wei, Z. (2015). Mechanism of Enhanced Humic Acid Removal from Aqueous Solution Using Poorly Crystalline Hydroxyapatite Nanoparti-cles. Dig. J. Nanomater. *Biostructures,* 10 663-680

[44] Astuti, W., Bendiyasa, I. M., Wahyuni, E. T., & Prasetya, A. (2010). The Effect of Coal Fly Ash Crystallinity toward Methyl Violet Adsorption Capacity. *ASEAN J. Chem.*, 10 8-14